Pharmacophore modeling and molecular docking analysis of glycyrrhizin as a potential anti-COVID-19 agent

Leyla Galandarli[1], Gulnara Akverdieva[2], Nurlan Amrahov[3], Rovshan Khalilov[4], and Afsun Sujayev[5]*

ABSTRACT

Traditional herbal medicines are widely used as complementary treatments for viral infections. Glycyrrhizin (GLR), a compound found in licorice root, has been proposed as a potential therapeutic agent for COVID-19. This study investigates the molecular interactions between GLR and two key severe acute respiratory syndrome coronavirus 2 (SARS-CoV-2) proteins—the main protease (M^{pro}) and the spike glycoprotein—using molecular docking simulations. Docking analyses were performed using AutoDock Vina, targeting SARS-CoV-2 M^{pro} (Protein Data Bank ID: 7ZQV) and the spike glycoprotein (Protein Data Bank ID: 6VXX). A site-specific docking approach was applied for all calculations. The binding sites were defined based on crystallized ligand-bound complexes, and a grid box of 40 × 40 × 40 points was applied for both receptors. The target proteins were kept rigid, while the ligand was allowed to remain flexible during both simulation procedures. The optimal conformation of the ligand was selected by ranking the binding energies of its poses according to the complex intermolecular interactions. PyMOL and Discovery Studio 3.1 were employed for visualization and interaction analysis. Results showed that GLR binds at the active site of the receptors, forming key interactions. The docking scores indicated strong binding affinities of −8.8 kcal/mol for the 7ZQV target and −9.5 kcal/mol for the 6VXX target, suggesting that GLR may serve as a potential inhibitor of these targets. Drawing on the derived computational findings, models of a pharmacophore for GLR binding to the specified receptors were proposed. These findings provide valuable insights into the molecular basis of GLR's antiviral activity and may guide the design of novel anti-COVID-19 therapeutics derived from natural compounds.

Keywords:

Glycyrrhizin; Severe acute respiratory syndrome coronavirus 2 main protease; Severe acute respiratory syndrome coronavirus 2 spike glycoprotein; Molecular docking; Pharmacophore model, COVID-19

***Corresponding author:**
Afsun Sujayev,
s.afsun@mail.ru

How to cite this article:
Galandarli L, Akverdieva G, Amrahov N, Khalilov R, Sujayev A. Pharmacophore modeling and molecular docking analysis of glycyrrhizin as a potential anti-COVID-19 agent. *Biomater Transl.* 2025.

doi: 10.12336/bmt.25.00117

1. Introduction

Identifying biological targets and elucidating the molecular mechanisms of drug action are a crucial task not only from the standpoint of fundamental science but also for the development of new, effective, and safe drugs. This understanding, supported by molecular docking and *in silico* absorption, distribution, metabolism, and excretion studies, enables optimization of therapeutic dosing regimens and helps prevent unexpected drug–drug interactions. However, it is important to note that the use of drugs containing certain reactive structural components with biological activity can be hazardous in some cases.[1,2]

Licorice root and its extracts have been used in traditional medicine to alleviate bronchitis, gastritis, and jaundice since ancient times. Licorice contains various phenolic compounds, including flavonoids, coumarins, and diphenylethanones, which contribute to its health benefits.[3-5] These compounds exhibit various pharmacological

effects, such as antioxidant, anti-inflammatory, and anticancer activities. For instance, glycybridins A-K, isolated from *Glycyrrhiza glabra*, exhibit diverse biological activities, including activation of nuclear factor erythroid 2-related factor 2, inhibition of tyrosinase and protein tyrosine phosphatase 1B, suppression of lipopolysaccharide-induced nitric oxide production, and inhibition of nuclear factor kappa B transcription. Moreover, glycybridin D demonstrated moderate cytotoxicity against human cancer cell lines and reduced tumor mass in a mouse model, with no significant systemic toxicity. In addition to these phenolic compounds, licorice also contains important triterpenoids, which play a key role in its wide range of biological activities. The most significant triterpenoid is glycyrrhizin (GLR), which gives licorice its sweet taste and contributes to its anti-inflammatory and antiviral properties.[6-10]

GLR is the calcium and potassium salt of the triterpenoid saponin glycyrrhizic acid, whose aglycone component is glycyrrhetinic acid. Chemically, GLR is a natural triterpenoid saponin designated as (3-β, 20-β)-20-carboxy-11-oxo-30-norolean-12-en-3-yl 2-O-β-d-glucopyranosyl-α-d-glucopyranosiduronic acid. As shown in **Figure 1A** and **B**, GLR comprises a hydrophilic part, two molecules of glucuronic acid, and a hydrophobic fragment, glycyrrhetinic acid. The molecular structure of GLR, with its numbered scheme, is shown in **Figure 1C**.

The antiviral, anticancer, anti-inflammatory, antitussive, antiosteoporotic, anti-Alzheimer's, antithrombotic, antidiabetic, antimicrobial, and antiallergic properties of GLR, as well as its positive protective effects on the human body as an antioxidant, hepatoprotective, cardioprotective, neuroprotective, antidepressant, immunomodulatory, and antiulcer agent, have been demonstrated.[11-27] Traditional herbal compounds have been considered promising candidates for the adjunctive treatment of viral infections and have recently gained attention in the context of COVID-19 therapy. The direct antiviral activity of glycyrrhizic acid against severe acute respiratory syndrome coronavirus 2 (SARS-CoV-2) has been demonstrated by researchers at the University of Duisburg-Essen and Ruhr University Bochum.[28] Their studies revealed that GLR, the principal bioactive constituent of licorice root, exhibits potent inhibitory effects on SARS-CoV-2 by targeting the viral main protease (M^{pro}), a key enzyme required for viral replication. Specifically, GLR was shown to suppress viral replication by blocking the enzymatic activity of M^{pro}, thereby preventing cleavage of viral polyproteins required for replication. This inhibition ultimately leads to viral inactivation. Due to its critical role in viral propagation, the M^{pro} remains one of the most extensively explored targets in anti-SARS-CoV-2 drug development. Recent literature increasingly supports the therapeutic potential of GLR against SARS-CoV-2 infection.[29-35] Notably, the coronavirus virion is spherical with spike-like projections on the envelope surface, composed of spike (S) glycoproteins, which are actively involved in the virus's fusion, entry into the host cell, and attachment. Its surface localization makes the S glycoprotein the main target for neutralizing antibodies and host immune responses. The S protein enables the enveloped virus to bind to host cells in the lower respiratory tract by forming homotrimers that protrude from the viral surface.[36-41] According to the literature review, a detailed study of the mechanism of action of GLR in treating COVID-19 has not been published to date.

This work is the first to thoroughly evaluate GLR as an anti-COVID-19 agent. The molecular docking method was used to investigate the interactions of this compound with the SARS-CoV-2 M^{pro} and the SARS-CoV-2 S glycoprotein. Moreover, the pharmacophore models of GLR and its derivatives for the interactions with the specified receptors were proposed.

2. Methodology

2.1. Calculation approaches

Molecular docking is a widely employed computational strategy in contemporary drug development for predicting binding affinities and interaction patterns between biologically active molecules and their receptors at the atomic level.[42-46] In the present research, this technique was applied to investigate the binding interactions of GLR with two major SARS-CoV-2 proteins, M^{pro} and the S glycoprotein, using AutoDock Vina software (version 1.5.6).[47] The molecular model of GLR was acquired from the ChemSpider repository (ID: 14263).[48] The three-dimensional crystal structures of the SARS-CoV-2 M^{pro} (Protein Data Bank ID: 7ZQV)[49] and the S glycoprotein (Protein Data Bank ID: 6VXX)[50] were obtained from the Research Collaboratory for Structural Bioinformatics Protein Data Bank. The binding sites within the target proteins were identified based on information from their respective ligand-bound crystal complexes. In both docking runs, a 40 × 40 × 40 Å grid was used to ensure the full coverage of the ligand-binding sites. Before docking, the co-crystallized compounds were removed from the receptor structure, and hydrogen atoms were subsequently introduced to complete the preparation. Kollman atomic charges were assigned to the proteins, while partial charges for the ligand were determined using the Gasteiger charge calculation method. The simulation kept the receptor fixed while allowing the ligand to move freely. Visualization and interaction analysis in both two and three dimensions were conducted using PyMOL (version 2.5.2) and Discovery Studio 3.1 tools.[51,52]

3. Results and discussion

To investigate the anti-COVID-19 properties of the GLR molecule, it was docked into the identified binding site of SARS-CoV-2 M^{pro} (7ZQV) and SARS-CoV-2 S glycoprotein (6VXX). The binding affinities and interaction modes were

[1]Department of "Young Talents" Lyceum, Baku State University, Baku, Azerbaijan, [2]Biophysics Division of Institute for Physical Problems, Baku State University, Baku, Azerbaijan, [3]Bioengineering SRL, The Center of Excellence in Research, Development, and Innovation, Baku State University, Baku, Azerbaijan, [4]Department of Biophysics and Biochemistry, Faculty of Biology, Baku State University, Baku, Azerbaijan, [5]Laboratory of Physiologically Active Organic Compounds of Institute of Chemistry of Additives, Azerbaijan National Academy of Sciences, Baku, Azerbaijan

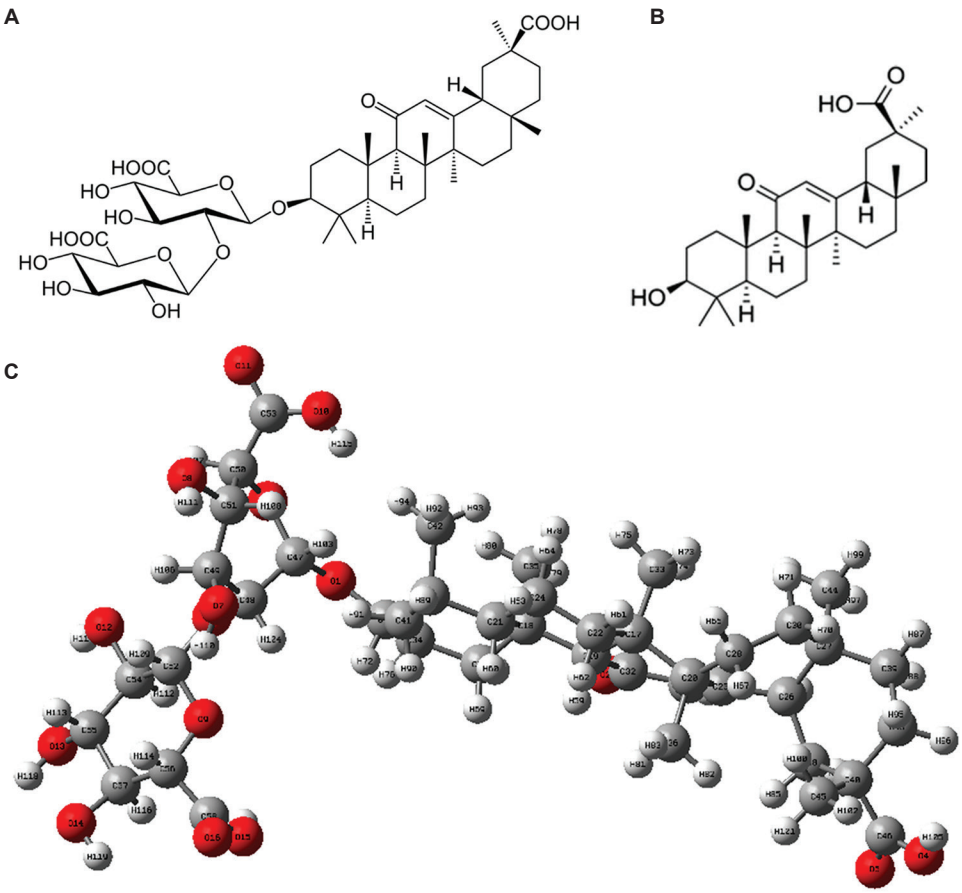

Figure 1. Chemical structure of (A) glycyrrhizin and its part (B) glycyrrhetinic acid, showing the atoms of the molecule in the order in which they are bonded. Molecular structure with (C) atomic numbering scheme for glycyrrhizin, showing the spatial arrangement of atoms within this molecule using a ball-and-stick model

then determined. To understand the stability of the minimized complexes, the important receptor-ligand interactions were visualized and analyzed. Docking results and detailed interaction analyses are presented in **Tables 1-4**, **Figures 2** and **3**. Significant interactions are illustrated with dotted lines. The results of the docking simulations are discussed individually for each target. The distances (Å) between the ligand's functional groups and the active site residues are also provided.

3.1. Molecular docking of GLR with 7ZQV

The strongest interaction found during docking showed that GLR binds to the SARS-CoV-2 M^{pro} with an energy of –8.8 kcal/mol. **Figure 2** illustrates both three-dimensional and two-dimensional representations of the important ligand 7ZQV contacts.

The analysis revealed that His41, Cys44, Ser46, Asn142, Gly143, His164, Thr190, and Gln192 functioned as active site residues for ligand binding in 7ZQV. The parameters of these contacts are presented in **Table 1**.

The hydrophilic regions of GLR primarily formed polar interactions with receptor residues, complemented by several van der Waals contacts. The His41 residue of the receptor B-chain participated in the electrostatic attraction and pi-donor hydrogen bonding with the terminal glucuronic ring of the ligand at distances of 5.59 and 2.24 Å, respectively. Ser46 formed unfavorable donor-donor interactions with the second glucuronic acid of the ligand, as well as two carbon–hydrogen bonds, at distances of 1.56 Å, 2.83 Å, and 3.20 Å, respectively. The Asn142 residue of the receptor was positioned to engage in 2.32- and 2.01-Å-long conventional hydrogen bonds with both glucuronic acids of this moiety. Cys44 and His164 amino acids of the receptor were involved in the intermolecular polar contacts with the hydrophilic part of the ligand by forming the conventional H-bonds at lengths of 2.76 and 2.41 Å, respectively. Notably, the terminal glucuronic acid of the ligand took part in the intermolecular unfavorable donor–donor interactions with Gly143 at a distance of 1.67 Å, but the terminal carboxyl group of the hydrophobic fragment formed unfavorable acceptor–acceptor interactions with Thr190 and unfavorable donor–donor interactions with Gln192 at distances of 2.95 Å and 1.69 Å, respectively. As observed, H-bonding played a crucial role in the interactions between the ligand and receptor, with GLR forming seven hydrogen bonds with the target residues. GLR's placement within the protein active site was also reinforced by van der Waals interactions involving Thr25, Thr45, Met49, Ser144, Cys145, His163, Met165, Gln166, Leu167, Pro168, Gln189, and Ala191 B-chain residues.

As observed from the presented results, the ligand established intermolecular contacts with Thr25, His41, Cys44, Thr45,

Table 1. The attributes of the glycyrrhizin-7ZQV intermolecular interactions

No	Interactions	Interaction type	Distances (Å)	Angle of DHA (°)	Angle of HAY (°)
1	GLR: H120-B: Asn142:OD1	Conventional HB	2.01	154.32	111.17
2	B: Asn142:HD22-GLR: O1	Conventional HB	2.32	156.64	108.34
3	GLR: H111-B: Cys44:O	Conventional HB	2.76	110.69	113.82
4	GLR: H119-B: His164:O	Conventional HB	2.41	119.77	114.68
5	GLR: H108-B: Ser46:OG	Carbon HB	3.20	118.52	113.10
6	B: Ser46:HA-GLR: O7	Carbon HB	2.83	123.17	112.67
7	B: Ser46:HG-GLR: H115	Unfavorable D-D	1.56	-	-
8	B: His41:NE2-GLR: O15	Attractive charge	5.59	-	-
9	GLR: H118-B: His41:O	Pi-D H-bond	2.24	-	-
10	B: Gly143:HN-GLR: H120	Unfavorable D-D	1.67	-	-
11	B: Thr190:O-GLR: O4	Unfavorable A-A	2.95	-	-
12	B: Gln192:HN-GLR: H105	Unfavorable D-D	1.69	-	-

Note: The ligand atom numbering is provided following **Figure 1C**.
Abbreviations: A: Acceptor; B: B-chain residue; D: Donor; GLR: Glycyrrhizin; H: Hydrogen; HB: Hydrogen bond; Y: Atom connected with the acceptor.

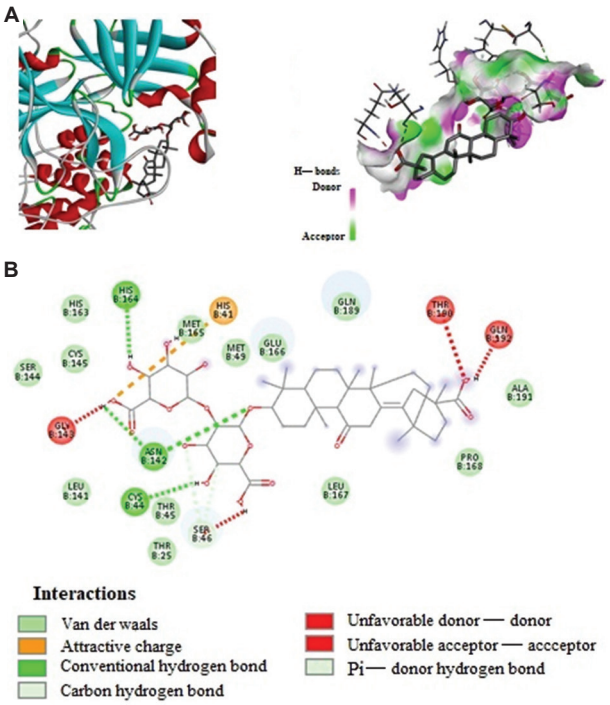

Figure 2. The molecular docking results of glycyrrhizin with 7ZQV. (A) Three-dimensional visualization and (B) two-dimensional diagram of the receptor–ligand interactions. The ligand and receptor are depicted, and important interactions, including hydrogen bonds, attractive charge interactions, and others, are highlighted

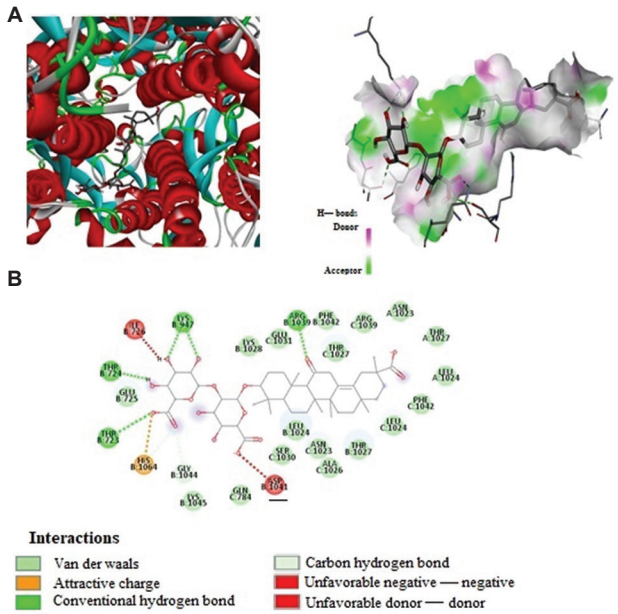

Figure 3. The molecular docking results of glycyrrhizin with 6VXX. (A) Three-dimensional visualization and (B) two-dimensional diagram of the receptor–ligand interactions. The ligand and receptor are depicted, and important interactions, including hydrogen bonds, attractive charge interactions, and others, are highlighted

Ser46, Met49, Asn142, Gly143, Leu141, Ser144, Cys145, His163, His164, Met165, Glu166, Leu167, Pro168, Gln189, Thr190, Ala191, and Gln192 residues of the receptor B-chain of SARS-CoV-2 M^{pro}. In addition, residues within the active site of the receptor also interacted with one another (**Table 2**). Thr25 took part in the intramolecular unfavorable acceptor–acceptor interactions with Cys44; in turn, Cys44 formed the intramolecular conventional hydrogen bonds with His41 and alkyl contacts with Met49. In addition, His41 participated in intramolecular unfavorable donor–donor and carbon–hydrogen bond interactions with His164, as well as in pi-sulfur interactions with Cys145. Residues Leu141 and Ser144 formed both conventional and carbon-hydrogen bonds with each other. His163 was positioned to engage in several carbon–hydrogen bonds with the Ser144 and Met165 residues, as well as both carbon-hydrogen bond and π-alkyl contacts with the Cys145 residue of the receptor. Conventional hydrogen bonds between Thr45 and Met49, Asn142 and Gly143, Leu141 and Ser144, Thr190 and Ala191, and carbon-hydrogen bonds between Met49 and Gln189, Pro168 and Gln192, located in the binding pocket of SARS-CoV-2 M^{pro}, were also formed. Therefore, the aforementioned receptor residues are crucial for binding with GLR, influencing the overall loop conformation and the stability of the complex.

Table 2. The parameters of the intramolecular interactions for the 7ZQV active site

No	Contacts	Interaction type	Distances (Å)
1	**B: Thr25:OG1–B: Cys44:O**	Unfavorable A–A	2.81
2	**B: His41:HD1–B: His164:HD1**	Unfavorable D–D	2.54
3	**B: His41:HE1–B: His164:O**	Carbon HB	2.62
4	**B: Cys44:HN–B: His41:O**	Conventional HB	2.05
5	**B: Cys44–B: Met49**	Alkyl	4.69
6	**B: Met49:HN–B: Thr45:O**	Conventional HB	2.87
7	**B: Gly143:HN–B: Asn142:OD1**	Conventional HB	2.34
8	**B: Ser144:HN–B: Leu141:O**	Conventional HB	2.38
9	**B: Ser144:HB1–B: Leu141:O**	Carbon HB	2.79
10	**B: Cys145:HA–B: His163:O**	Carbon HB	2.67
11	**B: Cys145:SG–B: His41**	Pi–sulfur	4.81
12	**B: His163–B: Cys145**	Pi–alkyl	5.16
13	**B: His163:HD2–B: Ser144:OG**	Carbon HB	3.06
14	**B: His163:HE1–B: Met165:O**	Carbon HB	2.58
15	**B: Pro168:HD1–B: Gln192:O**	Carbon HB	2.48
16	**B: Gln189:HN–B: Met49:O**	Carbon HB	1.70
17	**B: Ala191:HN–B: Thr190:OG1**	Conventional HB	2.12
18	B: Cys22:HN–**B: Thr25:O**	Conventional HB	1.90
19	**B: Thr25:HN**–B: Cys22:O	Conventional HB	2.46
20	**B: Thr25:HB**–B: Val42:O	Conventional HB	2.37
21	B: Asn28:HD22–**B: Gly143:O**	Conventional HB	2.47
22	**B: His41**–B: Pro39	Pi–alkyl	4.76
23	**B: Cys44**–B: Pro52	Alkyl	5.29
24	**B: Cys44**–B: Leu57	Alkyl	5.40
25	B: Pro52:HD1–**B: Met49:O**	Carbon HB	2.65
26	B: Tyr54–**B: Cys44**	Pi–alkyl	5.19
27	**B: Ser144:HA**–B: Cys117:O	Carbon HB	2.00
28	B: Ser147:HN–**B: Ser144:O**	Conventional HB	2.11
29	B: Tyr161:HH–**B: His163:HD1**	Unfavorable D–D	0.98
30	**B: His163**–B: Phe140	Pi–Pi stacked	3.65
31	**B: His164**–B: Cys85	Pi–alkyl	5.35
32	**B: His164**–B: Pro39	Pi–alkyl	4.33
33	**B: Met165:HN**–B: Ala173:O	Conventional HB	2.12
34	**B: His164:HD2**–B: Met162:O	Carbon HB	2.12
35	**B: His164:HN**–B: Ala173:O	Carbon HB	2.24
36	**B: Glu166**–B: Val171:O	Carbon HB	2.45
37	B: Thr169:HB–**B: Pro168:O**	Carbon HB	2.55
38	B: Gly170:HA1–**B: Glu166:OE2**	Carbon HB	2.53
39	B: Gly170:HN–**B: Leu167:O**	Conventional HB	2.18
40	B: Val171:HN–**B: Leu167:O**	Conventional HB	3.06
41	B: His172:HE2–**B: Glu166:OE1**	Salt bridge; attraction charge	2.49
42	B: Ala173:HN–**B: Leu167:O**	Alkyl	4.54
43	B: Phe185–**B: Leu167**	Pi–alkyl	4.84
44	B: Val186:HN–**B: Gln192:OE1**	Conventional HB	2.01
45	B: Arg188:HA–**B: Met49:O**	Carbon HB	3.01
46	**B: Thr190:HN**–B: Arg188:O	Conventional HB	2.46
47	**B: Gln192:HE22**–B: Val186:O	Conventional HB	2.13

Note: Amino acid residues that interact with the ligand are highlighted in bold.
Abbreviations: A: Acceptor; B: B-chain residue; D: Donor; HB: Hydrogen bond.

It was revealed that Cys22, Asn28, Pro39, Val42, Pro52, Tyr54, Leu57, Cys85, Cys117, Phe140, Ser147, Met162, Tyr161, Thr169, Gly170, Val171, His172, Ala173, Phe185, Val186, and Arg188 residues of the B-chain of the receptor may not be essential for the ligand–receptor contacts, but they stabilized the positions of the other receptor residues that were involved in the intermolecular interactions. As observed from the presented data (**Table 2**), these residues interacted with the receptor's active center residues through hydrogen bonding, alkyl, pi-alkyl, pi-pi stacking, and electrostatic contacts. Moreover, a salt bridge was formed between residues His172 and Glu166 due to the attraction of the opposing charges at a distance of 2.49 Å.

3.2. Molecular docking of GLR with 6VXX

The docking simulations of GLR with the SARS-CoV-2 S glycoprotein revealed a binding affinity of –9.5 kcal/mol. **Figure 3** shows three-dimensional and two-dimensional visualizations of key ligand-6VXX contacts.

The attributes of the GLR –6VXX intermolecular interactions are given in **Table 3**.

According to the results, the hydrophilic part of GLR was primarily responsible for binding to receptors. The terminal glucuronic acid was surrounded by hydrogen bonds on four sides. Conventional hydrogen bonds were formed between the oxygen atoms of the ligand and amino acid residues located in the B-chain of the protein, including Thr723 (2.94 Å), Thr724 (1.94 Å), and Lys947 (2.11 and 2.02 Å). The central part of the hydrophobic fragment, which is called glycyrrhetinic acid, also formed a conventional hydrogen bond with Arg1039 of the B-chain at a distance of 2.26 Å. Carbon–hydrogen bonds were also observed between the terminal hydrophilic carboxyl group of the ligand and B-chain receptor residues Gly1044 (2.46 Å) and His1064 (2.96 Å). In addition, electrostatic attractive charge interactions were observed between the ligand atom group and the His1064 residue of the receptor B-chain at a distance of 4.52 Å. The ligand's glucuronic acid groups engaged in unfavorable donor–donor contacts with Ile726 of the B-chain at 2.01 Å and in unfavorable negative–negative contacts with Asp1041 of the B-chain at 3.77 Å. The results further highlight the significance of hydrogen bonding in the binding of GLR to the SARS-CoV-2 S glycoprotein, where seven hydrogen bonds were formed. Notably, the ligand also formed van der Waals interactions with the next active site residues: Asn1023, Leu1024, and Thr1027 of the A-chain, Glu725; Leu1024, Thr1027, Lys1028, Phe1042, and Lys1045 of the B-chain; and Gln784, Asn1023, Leu1024, Ala1026, Thr1027, Ser1030, Glu1031, Arg1039, and Phe1042 of the C-chain.

The analysis showed that the active site residues involved in contacts with ligand, namely Asn1023, Leu1024, and Thr1027 of the A-chain; Thr723, Glu725, Lys947, Leu1024, Thr1027, Lys1028, Arg1039, Asp1041, Phe1042, Gly1044, Lys1045, and His1064 of the B-chain; and Gln784, Leu1024, Ala1026, Thr1027, Ser1030, Glu1031, Arg1039, and Phe 1042 residues of the C-chain also participated in intermolecular interactions among themselves (**Table 4**).

Table 3. The attributes of the glycyrrhizin-6VXX intermolecular interactions

No	Interactions	Interaction type	Distances (Å)	Angle of DHA (°)	Angle of HAY (°)
1	B: Thr723:HG1-GLR: O15	Conventional HB	2.94	96.64	117.00
2	GLR: H119-B: Thr724:O	Conventional HB	1.94	103.77	119.51
3	B: Ile726:HN-GLR: H118	Unfavorable, D–D	2.01	-	-
4	B: Lys947:HZ1-GLR: O13	Conventional HB	2.11	138.24	108.55
5	B: Lys947:HZ3-GLR: O12	Conventional HB	2.02	132.34	122.45
6	B: Arg1039:HH21-GLR: O2	Conventional HB	2.26	108.95	111.09
7	B: Asp1041:OD2-GLR: O10	Unfavorable, N–N	3.77	-	-
8	B: Gly1044:HA2-GLR: O16	Carbon HB	2.46	136.18	120.09
9	B: His1064:HD2-GLR: O16	Carbon HB	2.96	126.18	93.64
10	B: His1064:NE2-GLR: O15	Electrostatic, attractive charge	4.52	-	-

Note: The ligand atom numbering is provided following **Figure 1C**.
Abbreviations: A: Acceptor; B: B-chain residue; D: Donor; GLR: Glycyrrhizin; H: Hydrogen; HB: Hydrogen bond; N: Negative; Y: Atom connected with the acceptor.

A-chain Thr1027 formed conventional and carbon-hydrogen bonds with residues Asn1023 and Leu1024 of this receptor chain. In the B-chain, the Glu725 residue was involved in electrostatic attractive charge interactions with Lys947, Lys1028, and His1064, forming a salt bridge in the last contact. As demonstrated by the analysis, the B-chain residue Arg1039 occupied a central role in a network of conventional hydrogen bonds, electrostatic interactions, and salt-bridge attractive contacts with the Glu1031 residue of the C-chain. Concurrently, Glu1031 participated in both hydrogen bonding and electrostatic Pi-anion interactions with Thr1027 and Phe1042 of the C-chain, highlighting its key role in stabilizing the receptor–ligand interaction network. Symmetrical conventional bonding and pi-cationic interactions between Arg1039 and Phe1042 were observed in both the B- and C-chains of the receptor. Strong hydrogen bonds were formed in pairs between Thr723 and His1064, Asp1041 and Gly1044, Lys1028, and Phe1042 residues of the B-chain and between Gln784 and Ala1026 of the C-chain. Weak hydrogen bonds were formed in pairs between Thr1027 and Leu1024, Ser1030 and Thr1027 in both B and C-chains, between Ser1030 and Ala1026 residues of the C-chain, and between Lys1045 and Asp1041 of the B-chain. The analyzed contacts influenced the overall conformation of the binding pocket and the stability of the ligand-receptor complex.

Notably, the Lys1028 and Ser1030 residues of A-chain; Glu1031, Ser1037, Cys1032, Val1040, Cys1043, Ser1051, and Phe1062 of B-chain; and Ala1020, Ser1037, and Arg1019 residues of C-chain of the receptor may not be essential for the ligand–receptor contacts, but they took part in the formation of the hydrogen bonds, electrostatic interactions, salt bridges, pi–alkyl, and amide–pi stacked interactions with the active site residues Leu1024 and Thr1027 of A-chain; Lys1028, Arg1039 His1064 of B-chain; Asn1023, Ser1030, and Arg1039 of C-chain (**Table 4**).

Thus, it was demonstrated that the ligand bound to the active sites of both receptors through nonpolar, polar, and ionic interactions. As observed, GLR primarily participated in intermolecular hydrogen bonding and formed salt bridges with the receptor atoms. The high binding affinity against SARS-CoV-2 M^{pro} and SARS-CoV-2 S glycoprotein supports the hypothesis that GLR and its derivatives may serve as leads for anti-COVID-19 drug design.

We compared the molecular docking simulation results of GLR against 7ZQV and 6VXX receptors with similar studies. We report only residues overlapping the binding pockets that interact with the GLR molecule. The electron density maps of the crystallographic structures of AG7404 bound to both SARS-CoV-2 M^{pro} and SARS-CoV-1 M^{pro} and rupintrivir bound to SARS-CoV-2 M^{pro} showed clear densities corresponding to the inhibitors at the active sites. It was found that protein residues His41, Met49, Gly143, His163, His164, Glu166, Ser144, Cys145, Met165, Leu167, Gln189, and Thr190 interacting with the inhibitors were conserved between SARS-CoV-1 M^{pro} and SARS-CoV-2 M^{pro}, thereby suggesting that their efficacy as antivirals against both species might be similar.[49] According to the work by Liu and Wang,[53] the M^{pro} amino acids His41, Cys44, Met49, Ser144, Cys45, and Glu166 are predicted to play roles in drug interactions. On molecular docking, a number of ligands showed a remarkable binding affinity with the amino acids of SARS-CoV-2 M^{pro} receptor[54]: Rupintrivir with residues Glu166, Phe140, Gln189, Asn142, Ser46, Met49, and His41; ATN161 with residues Cys145, Ser144, His41, His164, Pro168, and Glu166; velpatasvir with residues Leu141, Gln189, Glu166, His41, Cys145, and Asn142; boceprevir with residues Gln189, Ser144, Phe140, Glu166, Met49, Met165, and His41; and ombitasvir with residues Gln189, Glu166, Cys145, His164, His41, and Ser46. As observed, the compounds occupied the same binding cavity as the reference compound, maintaining the interactions with conserved amino acid residues essential for significant inhibitory potential, especially for the compound velpatasvir, which showed the highest binding affinity. Notably, the velpatasvir molecule is structurally similar to the GLR molecule. Molecular docking studies of ERG tripeptide against M^{pro} revealed that SARS-CoV-2 M^{pro} amino acids His41, Asn142, Gly143, His163, His164, Glu166, Leu141, Cys145, and Met165 are the interacting amino acids.[55] It was found that the tetrandrine–M^{pro} receptor complex was stabilized by interacting with Thr25, His41, Ser46, Met49, Asn142, Cys145, Glu166, and Gln189.[56] Another ligand, aminopterin, interacted with Leu141, Asn142, Gly143,

Table 4. The parameters of the intramolecular interactions for the 6VXX active site

No	Contacts	Interaction types	Distances (Å)
1	**A: Thr1027:HG1–A: Asn1023:O**	Conventional HB	2.03
2	**A: Thr1027:HN–A: Asn1023:O**	Conventional HB	1.97
3	**A: Thr1027:HB–A: Leu1024:O**	Carbon HB	2.53
4	**B: Thr723:HN–B: His1064:O**	Conventional HB	2.02
5	**B: Lys947:NZ–B: Glu725:OE2**	Electrostatic, attractive charge	5.50
6	**B: Thr1027:HB–B: Leu1024:O**	Carbon HB	2.53
7	**B: Lys1028:NZ–B: Glu725:OE1**	Electrostatic, attractive charge	3.72
8	**B: Lys1028:HZ1–B: Phe1042:O**	Conventional HB	1.84
9	**B: Lys1028:HZ2–B: Phe1042**	Pi–cation	3.05
10	**B: Ser1030:HB–B: Thr1027:O**	Carbon HB	2.81
11	**B: Arg1039:NH1–B: Phe1042**	Pi–cation	3.65
12	**B: Arg1039:HE–C: Glu1031:OE1**	Conventional HB	2.03
13	**B: Arg1039:NH1–C: Glu1031:OE1**	Electrostatic, attractive charge	5.10
14	**B: Arg1039:H–C: Glu1031:OE1**	Salt bridge, attractive charge	2.01
15	**B: Asp1041:HA–B: Gly1044:O**	Carbon HB	2.36
16	**B: His1064:HE2–B: Glu725:OE1**	Salt bridge, attractive charge	1.93
17	**B: His1064: HN–B: Thr723:O**	Conventional HB	1.86
18	**B: Phe1042:HN–B: Arg1039:O**	Conventional HB	2.35
19	**C: Glu1031:HN–C: Thr1027:O**	Conventional HB	1.89
20	**C: Gln784:HE22–C: Ala1026:O**	Conventional HB	2.07
21	**C: Thr1027:HB–C: Leu1024:O**	Carbon HB	2.53
22	**C: Ser1030:HN–C: Thr1027:O**	Carbon HB	2.77
23	**C: Ser1030:HN–C: Ala1026:O**	Carbon HB	2.14
24	**C: Glu1031:OE1–C: Phe1042**	Electrostatic, pi–anion	5.00
25	**C: Arg1039:NH1…C: Phe1042**	Pi–cation	3.65
26	**C: Phe1042:HN…C: Arg1039:O**	Conventional HB	2.35
27	**B: Lys1045:H…B: Asp1041:OD1**	Carbon HB	2.60
28	**B: Thr724:HA**–B: Phe1062:O	Carbon HB	2.39
29	**B: Arg1039:H**–B: Glu1031:OE2	Salt bridge, charge–charge	2.05
30	**B: Arg1039:HD1**–B: Glu1031:OE1	Carbon HB	3.02
31	**B: Arg1039:HH12**–B: Glu1031:OE1	Salt bridge, charge–charge	2.01
32	**B: Arg1039:H**–B: Ser1037:OG	Conventional HB	2.20
33	**B: Arg1039:HN**–C: Ser1037:OG	Conventional HB	2.20
34	B: Ser1037:HG–**B: Arg1039:O**	Conventional HB	2.98
35	**B: His1064**–B: Cys1032	Pi–alkyl	4.42
36	**B: His1064:H**–B: Ser1051:OG	Carbon HB	2.55
37	B: Glu1031:HN–**B: Lys1028:O**	Conventional HB	2.67
38	B: Cys1043:C–**B: His1064**	Amide–pi stacked	3.78
39	B: Cys1032:HN–**B: Lys1028:O**	Conventional HB	2.28
40	A: Ser1030:HN–**A: Thr1027:O**	Conventional HB	2.77
41	A: Lys1028:HN–**A: Leu1024:O**	Carbon HB	1.90
42	**C: Asn1023:HN**–C: Arg1019:O	Conventional HB	1.88
43	**C: Leu1024:HN**–C: Ala1020:O	Conventional HB	2.04
44	**C: Ser1030:HB2**–B: Val1040:O	Carbon HB	2.46
45	C: Ser1037:HG–**C: Arg1039:O**	Conventional HB	2.98

(*Contd...*)

Table 4. (*Continued*)

Note: Amino acid residues that interact with the ligand are highlighted in bold.
Abbreviations: A: A-chain residue; B: B-chain residue; C: C-chain residue; D: Donor; HB: Hydrogen bond.

Cys145, and Gln189 amino acid residues of the M^{pro}.[57] From the fragment molecular orbital study-based interaction analysis on a complex between the SARS-CoV-2 M^{pro} and its peptide-like inhibitor, His41, His163, His164, and Glu166 were found to be the most important interacting amino acid residues, mainly due to hydrogen bonding with the inhibitor.[58] The interactions of succinic acid with Ser144, Cys145, and Glu166 amino acid residues of the M^{pro} were also revealed by molecular docking studies.[59] In previous studies,[60-62] the number of bioactive compounds found in medicinal plants, including GLR and its derivatives, was assessed as potential inhibitors of the COVID-19 M^{pro}. Using a molecular docking study, it was demonstrated that the His41, Ser46, Asn142, Gly143, Cys145, His163, His164, and Glu166 residues form the active site pocket of the M^{pro}. As shown, the results of the GLR –SARS-CoV-2 M^{pro} interaction in this study are consistent with the aforementioned literature data.

The molecular docking results of GLR against the SARS-CoV-2 S glycoprotein were also compared with the literature. It was found that Asn1023, Thr1027, Lys1028, Asp1041, and Phe1042 are interacting amino acids in the molecular docking simulations of ERQ tripeptide against S glycoprotein.[55] The molecular docking study revealed that the cepharanthine molecule interacted with the amino acid residues Glu725, Gln784, Ala1026, Asp1041, Phe1042, and Lys1045 of the S glycoprotein.[63] Amentoflavones also formed hydrogen bonds with Arg1039 and Asn1023.[64] As shown by Holanda *et al.*,[65] the residues Asp1041 and Leu1049 have a significant attraction for the anti-SARS-CoV-2 ligands. The indicated works confirm the calculated results of GLR interactions with the SARS-CoV-2 S glycoprotein.

3.3. Pharmacophore models of GLR for interactions with 7ZQV and 6VXX

In this study, models for the interaction of the pharmacophore moieties of GLR with 7ZQV and 6VXX were developed. To achieve this, the GLR conformations from both docking procedures were analyzed. The data suggested that the pharmacophore properties of GLR are highly compatible with the shape and chemistry of the receptor binding pockets. As shown in **Figure 4A**, GLR adopted a compact conformation in the cavity of 7ZQV, in which its terminal glucuronic acid folded toward its hydrophobic region. Within the aliphatic part, a strong (H110 O12) contact was particularly notable. This interaction occurred at a distance of 2.51 Å, with angles

of 136.66° (DHA) and 104.33° (HAY). In this conformation, mainly hydrogen atoms of the aliphatic part of the ligand participated in hydrogen bonding contacts with the receptor. In contrast, the binding pocket of the SARS-CoV-2 S glycoprotein forms a deep channel created by its trimeric structure, resulting in a more extended structure of the ligand (**Figure 4B**). In this arrangement, the aliphatic moiety engaged in hydrogen bonding, while the hydrophobic region participated in an attractive electrostatic interaction with the receptor.

Analysis of the structure–activity relationship data revealed that the carboxyl groups (-COOH), hydroxyl groups (-OH), ketone groups (=O), and ether groups (-O-) of GLR and its analogs are crucial for binding to SARS-CoV-2-19-related proteins.[66,67] Utilizing these insights alongside the computational results obtained, pharmacophore models depicting GLR's binding to SARS-CoV-2 M^{pro} and S glycoprotein were constructed and are illustrated in **Figures 5** and **6**, respectively.

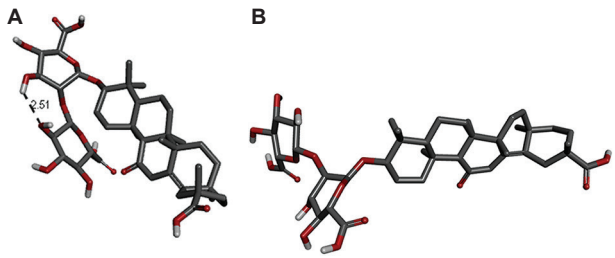

Figure 4. The optimal three-dimensional structure of glycyrrhizin corresponding to the best binding pose in the active site of the (A) severe acute respiratory syndrome coronavirus 2 (SARS-CoV-2) main protease (7ZQV) and (B) SARS-CoV-2 spike glycoprotein (6VXX), determined through molecular docking simulation

As shown in **Figure 5**, the pharmacophore centers of GLR interacting with SARS-CoV-2 M^{pro} include O15 and H120 of the –COOH group; H118 and H119 of the carbonyl groups in the terminal glucuronic acid; O7 and H111 of additional carbonyl groups; H108 of the aromatic C–H group; H115 of the subsequent glucuronic acid's –COOH group; O4 and H105 of the –COOH group at the glycyrrhetinic acid terminus; and O1 of the ether linkage connecting the hydrophilic and hydrophobic fragments.

As shown in **Figure 6**, O15 and O16 atoms of the carboxyl group, H118, H119, O12, and O13 atoms of the carbonyl groups, O10 atom of the COOH group in the sequence of the hydrophilic part, and O2 atom of the ketone part of the glycyrrhetinic acid served as the pharmacophore centers of GLR for its intermolecular interactions with the SARS-CoV-2 S glycoprotein. The spatial arrangement of GLR's pharmacophore regions for interactions with 7ZQV and 6VXX was quantified by a series of inter-feature distances, which are summarized in **Tables 5** and **6**, respectively. The

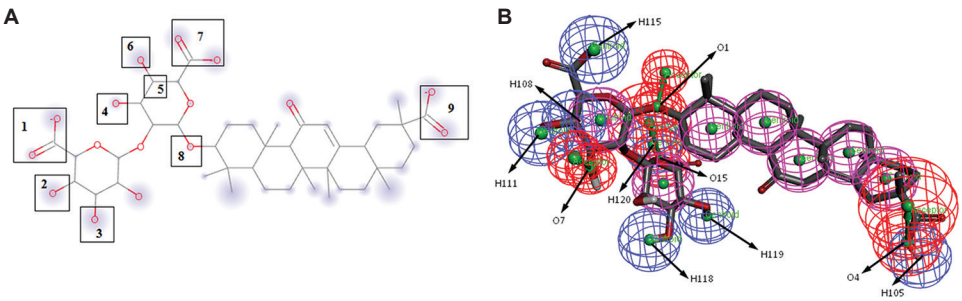

Figure 5. A pharmacophore model of glycyrrhizin, highlighting functional groups involved in the interaction with the 7ZQV target protein. (A) Pharmacophore moieties are marked with numbers: 1, 7, 9 for carboxyl groups (–COOH), 2, 3, 4, and 6 for hydroxyl groups (–OH), 8 for the ether group (–O–), and 5 for the aromatic CH group. (B) A pharmacophore model of glycyrrhizin showing H-acceptors in red, H-donors in blue, hydrophobic groups in violet, and their centers are indicated by labels and symbols

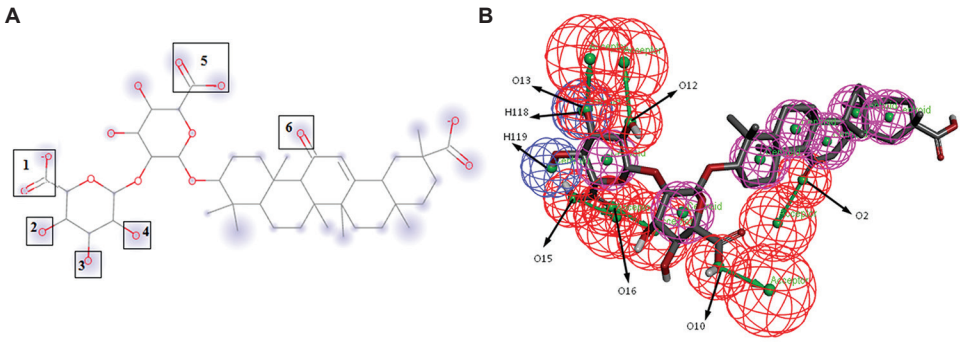

Figure 6. A pharmacophore model of glycyrrhizin, highlighting functional groups involved in the interaction with the 6VXX target protein. (A) Pharmacophore moieties are marked with numbers: 1, 5 as carboxyl groups (COOH); 2, 3, and 4 as hydroxyl radicals (OH), and 6 as a ketone group (=O). (B) A pharmacophore model of glycyrrhizin showing H-acceptors in red, H-donors in blue, hydrophobic groups in violet, and their centers are indicated by labels and symbols

Table 5. The respective geometrical arrangement of the pharmacophore centers of glycyrrhizin for connection with 7ZQV

Connections	Distance (Å)	Connections	Distance (Å)
O1-O4	13.77	H111-O4	17.86
O1-O7	4.76	H115-O4	17.29
O1-O15	5.99	H118-O4	12.95
O4-O7	15.33	H119-O4	11.42
O4-O15	14.75	H118-O7	5.82
O7-O15	8.11	H119-O7	8.71
H111-O1	6.08	H118-O15	5.65
H115-O1	4.44	H119-O15	4.19
H118-O1	6.90	H118-H111	8.39
H119-O1	7.41	H119-H111	11.20

Table 6. The respective geometrical arrangement of the pharmacophore centers of glycyrrhizin for connection with 6VXX

Connections	Distance (Å)	Connections	Distance (Å)
O2-O10	9.62	O13-O15	5.35
O2-O13	12.87	O13-O16	5.77
O2-O15	12.76	H118-O2	12.93
O7-O15	8.39	H119-O2	13.92
O2-O16	10.80	H118-O10	11.29
O2-O12	11.28	H119-O10	10.90
O10-O12	8.49	H118-O12	3.73
O10-O13	10.79	H119-O12	5.67
O10-O15	10.01	H118-O15	4.93
O10-O16	8.39	H119-O15	2.23
O12-O15	6.51	H118-O16	5.51
O12-O16	6.08	H119-O16	3.87

proposed models can be useful for the development of new GLR derivative compounds for medical applications.

4. Conclusion

Molecular docking studies of GLR revealed that this compound formed a stable complex with SARS-CoV-2 protein targets. It was shown that GLR formed key interactions with His41, Cys44, Ser46, Asn142, Gly143, His 164, Thr190, and Gln 192 residues of the binding pocket of SARS-CoV-2 M^{pro} (7ZQV) and with Thr723, Thr724, ILE726, Lys947, Arg 1039, Asp1041, Gly1044, and His1064 residues of the binding pocket of the of SARS-CoV-2 S glycoprotein (6VXX). The main attributes of the intermolecular interactions were computed. The effects of the intermolecular hydrogen bonding on the stability of the receptor–ligand complex were observed in both cases: GLR formed numerous hydrogen bonds with the target residues. Utilizing the derived results, pharmacophore models for the binding of GLR with the specified receptors were proposed. We characterized the spatial arrangement of GLR's binding regions on 7ZQV and 6VXX using pharmacophore distances. The results indicate that GLR is a promising antiviral candidate, warranting further investigation for the treatment of COVID-19.

Acknowledgement
None.
Financial support
None.
Conflicts of interest statement
The authors declare no conflicts of interest.
Author contributions
Conceptualization: LG, GA, AS; *Formal analysis*: LG, GA; *Investigation:* LG, GA; *Methodology*: GA; *Software:* LG, NA; *Writing – original draft*: LG, GA; *Writing – review & editing*: RK, AS. All authors have read and agreed to the published version of the manuscript
Ethics approval and consent to participate
Not applicable.
Consent for publication
Not applicable.
Availability of data
All data analyzed have been presented in the paper.

References

1. Demir Y. Naphthoquinones, benzoquinones, and anthraquinones: Molecular docking, ADME and inhibition studies on human serum paraoxonase-1 associated with cardiovascular diseases. *Drug Dev Res.* 2020;81(6):628-636. doi: 10.1002/ddr.21667
2. Demir Y. Exploring the inhibitory effects of quinolone medications on carbonic anhydrase enzyme activity: *In vitro* and *in silico* investigation. *Chem Select.* 2024;9(30):2365-6549. doi: 10.1002/slct.202402129
3. Özdemir K, Demir Y. Phenolic compounds in exercise physiology: Dual role in oxidative stress and recovery adaptation. *Food Sci Nutr.* 2025;13(8):e70714. doi: 10.1002/fsn3.70714
4. Ji X, Liu N, Huang S, Zhang C. A comprehensive review of licorice: The preparation, chemical composition, bioactivities and its applications. *Am J Chin Med.* 2024;52(3):667-716. doi: 10.1142/S0192415X24500289
5. Wu Y, Wang Z, Du Q, *et al.* Pharmacological effects and underlying mechanisms of licorice-derived flavonoids. *Evid Based Complement Alternat Med.* 2022;2022:9523071. doi: 10.1155/2022/9523071
6. Ploeger B, Mensinga T, Sips A, Seinen W, Meulenbelt J, DeJongh J. The pharmacokinetics of glycyrrhizic acid evaluated by physiologically based pharmacokinetic modeling. *Drug Metab Rev.* 2001;33(2):125-147. doi: 10.1081/DMR-100104400
7. Moustafa GO, Shalaby A, Naglah AM, Mounier MM, Anwar MM, Nossier ESS. Synthesis, characterization, *in vitro* anticancer potentiality, and antimicrobial activities of novel peptide-glycyrrhetinic-acid-based derivatives. *Molecules.* 2020;26(15):4573. doi: 10.3390/molecules26154573
8. Fujii S, Tuvshintogtokh I, Mandakh B, *et al.* Screening of *Glycyrrhiza uralensis* Fisch. ex DC. Containing high concentrations of glycyrrhizin by Eastern blotting and enzyme-linked immunosorbent assay using anti-glycyrrhizin monoclonal antibody for selective breeding of licorice. *J Nat Med.* 2014;68(4):717-722. doi: 10.1007/s11418-014-0847-7
9. Ming LJ, Yin AC. Therapeutic effects of glycyrrhizic acid. *Nat Prod Commun.* 2013;8(3):415-418.
10. Shajini BY, Krishnan D, Dev BS, *et al.* Potential benefits of *Glycyrrhiza glabra* (Liquorice) herb, its chemical make-up and significance in safeguarding poultry health: Current scientific knowledge. *J Exp Biol Agric Sci.* 2023;11(3):462-478. doi: 10.18006/2023.11(3).462.478

11. Yang R, Yuan BC, Ma YS, Zhou S, Liu Y. The anti-inflammatory activity of licorice, a widely used Chinese herb. *Pharm Biol.* 2017;55(1):5-18. doi: 10.1080/13880209
12. Shah SL, Wahid F, Khan N, *et al.* Inhibitory effects of *Glycyrrhiza glabra* and its major constituent glycyrrhizin on inflammation-associated corneal neovascularization. *Evid Based Complement Alternat Med.* 2018;2018:8438101. doi: 10.1155/2018/8438101
13. Shiba F, Miyauchi M, Chea C, *et al.* Anti-inflammatory effect of glycyrrhizin with *Equisetum arvense* extract. *Odontology.* 2021;109(2):464-473. doi:10.1007/s10266-020-00563-3
14. Leite CDS, Bonafé GA, Carvalho Santos J, Martinez CAR, Ortega MM, Ribeiro ML. The anti-inflammatory properties of licorice (*Glycyrrhiza glabra*)-derived compounds in intestinal disorders. *Int J Molecular Sci.* 2022;23(8):4121. doi: 10.3390/ijms23084121
15. Li C, Li L, Lan T. Co-treatment with disulfiram and glycyrrhizic acid suppresses the inflammatory response of chondrocytes. *J Orthop Surg* Res. 2021;16(1):132. doi: 10.1186/s13018-021-02262-3
16. Ashfaq UA, Masoud MS, Nawaz Z. Glycyrrhizin as an antiviral agent against hepatitis C virus. *J Transl Med.* 2011;9(1):112. doi: 10.1186/1479-5876-9-112
17. Nada F, Abo El-Magd A, Amro El-Karef M, El-Shishtawy MM, Eissa LA. Hepatoprotective effects of glycyrrhizin and omega-3 fatty acids on nuclear factor-kappa B pathway in thioacetamide-induced fibrosis in rats. *Egypt J Basic Appl Sci.* 2015;2(2):65-74. doi: 10.1016/j.ejbas.2014.12.005
18. Li JY, Cao HY, Liu P, Cheng GH, Sun MY. Glycyrrhizic acid in the treatment of liver diseases: Literature review. *Biomed Res Int.* 2014;2014:872139. doi: 10.1155/2014/872139
19. Xu F, Huang X, Wu H, Wang X. Screening compounds for treating the diabetes and COVID-19 from Miao medicine by molecular docking and bioinformatics. *Arab J Chem.* 2023;16(9):105001. doi: 10.1016/j.arabjc.2023.105001
20. Baltina LA, Tasi YT, Huang SH, *et al.* Glycyrrhizic acid derivatives as dengue virus inhibitors. *Bioorg Med Chem Lett.* 2019;29(20):126645. doi: 10.1016/j.bmcl.2019.126645
21. Wolkerstorfer A, Kurz H, Bachhofner N, Szolar OH. Glycyrrhizin inhibits influenza A virus uptake into the cell. *Antiviral Res.* 2009;83(2):171-178. doi: 10.1016/j.antiviral.2009.04.012
22. Han S, Sun L, He F, Che H. Anti-allergic activity of glycyrrhizic acid on IgE-mediated allergic reaction by regulation of allergy-related immune cells. *Sci Rep.* 2017;7(1):7222. doi: 10.1038/s41598-017-07833-1
23. Sharma R, Santosh K, Guru S, *et al.* 3-(2,6-Dichloro-benzyloxy)-11-oxo-olean-12-ene-29-oic acid, a semisynthetic derivative of glycyrrhetic acid: Synthesis, antiproliferative, apoptotic, and anti-angiogenesis activity. *Med Chem Commun.* 2015;6:564. doi: 10.1039/b000000x
24. Ahmad A, Tiwari RK, Mishra P, *et al.* Antiproliferative and apoptotic potential of glycyrrhizin against HPV16^{+} Caski cervical cancer cells: A plausible association with downregulation of HPV E_6 and E_7 oncogenes and Notch signaling pathway. *Saudi J Biol Sci.* 2022;29(5):3264-3275. doi: 10.1016/j.sjbs.2022.01.054
25. Cheng X, Liu Y, Qi B, *et al.* Glycyrrhizic acid alleviated MI/R-induced injuries by inhibiting Hippo/YAP signaling pathways. *Cell Signal.* 2024;115:111036. doi: 10.1016/j.cellsig.2024.111036
26. Yamamoto M, Nagasawa Y, Fujimori K. Glycyrrhizic acid suppresses the early stage of adipogenesis through repression of MEK/ERK-mediated C/EBPβ and C/EBPδ expression in 3T3-L1 cells. *Chem Biol Interact.* 2021;346:109595. doi: 10.1016/j.cbi.2021.109595
27. Lv X, Zhu Y, Deng Y, *et al.* Glycyrrhizin improved autophagy flux via HMGB1-dependent Akt/mTOR signaling pathway to prevent doxorubicin-induced cardiotoxicity. *Toxicology.* 2020;441:152508. doi: 10.1016/j.tox.2020.152508
28. Van De Sand L, Bormann M, Alt M, *et al.* Glycyrrhizin effectively inhibits SARS-CoV-2 replication by inhibiting the viral main protease. *Viruses.* 2021;13(4):609. doi: 10.3390/v13040609
29. Maddah M, Bahramsoltani R, Hoseini YN, Rahimi R, Aliabadi R, Pourfath M. Proposing high-affinity inhibitors from *Glycyrrhiza glabra* L. Against SARS-CoV-2 infection: Virtual screening and computational analysis. *New J Chem.* 2021;45:15977-15995. doi: 10.1039/D1NJ02031E
30. Banerjee S, Baidya SK, Adhikari N, Ghosh B, Jha T. Glycyrrhizin as a promising kryptonite against SARS-CoV-2: Clinical, experimental, and theoretical evidences. *J Mol Struct.* 2023;1275:134642. doi: 10.1016/j.molstruc.2022.134642
31. Gomaa AA, Abdel-Wadood YA, Gomaa MA. Glycyrrhizin and boswellic acids, the golden nutraceuticals: Multitargeting for treatment of mild-moderate COVID-19 and prevention of post-COVID cognitive impairment. *Inflammopharmacol.* 2022;30(6):1977-1992. doi: 10.1007/s10787-022-01062-3
32. Bijelić K, Hitl M, Kladar N. Phytochemicals in the prevention and treatment of SARS-CoV-2-clinical evidence. *Antibiotics (Basel).* 2022;11(11):1614. doi: 10.3390/antibiotics11111614
33. Zhang B, Qi F. Herbal medicines exhibit a high affinity for ACE2 in treating COVID-19. *Biosci Trends.* 2023;17(1):14-20. doi: 10.5582/bst.2022.01534
34. He MF, Liang JH, Shen YN, *et al.* Glycyrrhizin inhibits SARS-CoV-2 entry into cells by targeting ACE2. *Life (Basel).* 2022;12(11):1706. doi: 10.3390/life12111706
35. Antonopoulou I, Sapountzaki E, Rova U, Christakopoulos P. Inhibition of the main protease of SARS-CoV-2 (Mpro) by repurposing/designing drug-like substances and utilizing nature's toolbox of bioactive compounds. *Comput Struct Biotechnol J.* 2022;20:1306-1344. doi: 10.1016/j.csbj.2022.03.009
36. Lei R, Qing E, Odle A, *et al. Functional and Antigenic Characterization of SARS-CoV-2 Spike Fusion Peptide by Deep Mutational Scanning. bioRxiv* [Preprint]; 2023. doi: 10.1101/2023.11.28.569051
37. Garrett ME, Galloway JG, Wolf C, *et al.* Comprehensive characterization of the antibody responses to SARS-CoV-2 spike protein finds additional vaccine-induced epitopes beyond those for mild infection. *Elife.* 2022;11:e73490. doi: 10.7554/eLife.73490
38. Laporte M, Raeymaekers V, Van Berwaer R, *et al.* The SARS-CoV-2 and other human coronavirus spike proteins are fine-tuned towards temperature and proteases of the human airways. *PLoS Pathog.* 2021;17(4):e1009500. doi: 10.1371/journal.ppat.1009500
39. Pillaiyar T, Meenakshisundaram S, Manickam M. Recent discovery and development of inhibitors targeting coronaviruses. *Drug Discov Today.* 2020;25(4):668-688. doi: 10.1016/j.drudis.2020.01.015
40. Johnson MC, Lyddon TD, Suarez R, *et al.* Optimized pseudotyping conditions for the SARS-COV-2 spike glycoprotein. *J Virol.* 2020;94(21):e01062-20. doi: 10.1128/JVI.01062-20
41. Takeda M. Proteolytic activation of SARS-CoV-2 spike protein. *Microbiol Immunol.* 2021;66(1):15-23. doi: 10.1111/1348-0421.12945
42. Karağaç MS, Yeşilkent EN, Kizir D, *et al.* Esculetin improves inflammation of the kidney via gene expression against doxorubicin-induced nephrotoxicity in rats: *In vivo* and *in silico* studies. *Food Biosci.* 2024;62:105159. doi: 10.1016/j.fbio.2024.105159
43. Demir Y, Öztürk N, Isıyel M, Ceylan H. Effects of carnosic and usnic acid on pentose phosphate pathway enzymes: An experimental and molecular docking study. *Chem Select.* 2024;9(27):e202401067. doi: 10.1002/slct.202401067
44. Sever B, Altıntop MD, Demir Y, *et al.* Identification of a new class of potent aldose reductase inhibitors: Design, microwave-assisted synthesis, *in vitro* and *in silico* evaluation of 2-pyrazolines. *Chem Biol*

Interact. 2021;345:109576.
doi: 10.1016/j.cbi.2021.109576

45. Tahirli S, Aliyeva F, Şenol H, *et al.* Novel complex compounds of nickel with 3-(1-phenyl-2,3-dimethyl-pyrazolone-5)azopentadione-2,4: Synthesis, NBO analysis, reactivity descriptors and *in silico* and *in vitro* anti-cancer and bioactivity studies. *J Biomol Struct Dyn.* 2024;43:5552-5576.
doi: 10.1080/07391102.2024.2309646
46. Galandarli L, Akverdieva G. Molecular docking evaluation of glycyrrhizin as anti-stress and anti-diabetic agent. *New Mater Compd Appl.* 2025;9(2):223-239.
doi: 10.62476/nmca.92223
47. Trott O, Olson AJ. AutoDock Vina: Improving the speed and accuracy of docking with a new scoring function, efficient optimization, and multithreading. *J Comput Chem.* 2010;31(2):455-461.
doi: 10.1002/jcc.21334
48. Yonekura-Sakakibara K, Saito K. Functional genomics for plant natural product biosynthesis. *Nat Prod Rep.* 2009;26:1466-1487.
doi: 10.1039/B817077K
49. Fàbrega-Ferrer M, Herrera-Morandé A, Muriel-Goñi S, *et al.* Structure and inhibition of SARS-CoV-1 and SARS-CoV-2 main proteases by oral antiviral compound AG7404. *Antiviral Res.* 2022;208:105458.
doi: 10.1016/j.antiviral.2022.105458
50. Walls AC, Park Y, Tortorici MA, Wall A, McGuire AT, Veesler D. Structure, function, and antigenicity of the SARS-CoV-2 spike glycoprotein. *Cell.* 2020;181(2):281-292.e6.
doi: 10.1016/j.cell.2020.02.058
51. DeLano WL. *The PyMOL Molecular Graphics System*; 2010. Available from: https://www.ccp4.ac.uk/newsletters/newsletter40/11_pymol.pdf [Last accessed on 2025 Oct 30].
52. Discovery Studio 3.1. *Discovery Studio Visualization.* Available from: https://accelrys.com/products/collaborative/science/biovia/discovery/studio/visualization-download.php [Last accessed on 2016 Dec 02].
53. Liu X, Wang XJ. Potential inhibitors against the 2019-nCoV coronavirus M protease from clinically approved medicines. *J Genet Genomics.* 2020;47(2):119-121.
doi: 10.1016/j.jgg.2020.02.001
54. Chaurasiya A, Shome A, Chawla PA. Molecular docking analysis of peptide-based antiviral agents against SARS-CoV-2 main protease: An approach towards drug repurposing. *Explor Med.* 2023;4:33-44.
doi: 10.37349/emed.2023.00123
55. Yılmaz G, Çelik S, Erbölükbaş Özel A, Akyüz S. *In silico* evaluation of ERQ bioactive tripeptide as an anticancer agent and an inhibitor of SARS-CoV-2 enzymes. *Eur J Biol.* 2024;83:34-41.
doi: 10.26650/EurJBiol.2024.1389569
56. Begum SKA, Begum S, Bandari P, Swapna BS, Reddemma MT. Tetrandrine, an effective inhibitor of COVID-19 main protease (M^{pro}); Insights from molecular docking and dynamics simulations. *Int J Pharm Investig.* 2023;13(4):845-851.
doi: 10.5530/ijpi.13.4.106
57. Çelik S, Yılmaz G, Akyüz S, Özel AE. Shedding light on the biological activity of aminopterin, via molecular structural, docking, and molecular dynamics analyses. *J Biomol Struct Dyn.* 2023;1-22.
doi: 10.1080/07391102.2023.2245493
58. Hatada R, Okuwaki K, Mochizuki Y. Fragment molecular orbital-based interaction analyses on COVID-19 main protease - inhibitor N3 complex (PDB ID: 6LU7). *J Chem Inf Model.* 2020;60(7):3593-3602.
doi: 10.1021/acs.jcim.0c00283
59. Sagaama A, Brandan SA, Ben Issa T, Issaoui N. Searching potential antiviral candidates for the treatment of the 2019 novel coronavirus based on DFT calculations and molecular docking. *Heliyon.* 2020;6(8):e04640.
doi: 10.1016/j.heliyon.2020.e04640
60. Khaerunnisa S, Kurniawan H, Awaluddin R, Suhartati S, Soetjipto S. *Potential Inhibitor of COVID-19 Main Protease (Mpro) from Several Medicinal Plant Compounds by Molecular Docking Study.* [Preprint]; 2020.
doi: 10.20944/preprints202003.0226.v1
61. Rai H, Barik A, Singh YP, *et al.* Molecular docking, binding mode analysis, molecular dynamics, and prediction of ADMET/toxicity properties of selective potential antiviral agents against SARS-CoV-2 main protease: An effort toward drug repurposing to combat COVID-19. *Mol Divers.* 2021;25:1905-1927.
doi: 10.1007/s11030-021-10188-5
62. Srivastava V, Yadav A, Sarkar P. Molecular docking and ADMET study of bioactive compounds of *Glycyrrhiza glabra* against main protease of SARS-CoV2. *Mater Today Proc.* 2022;49(8):2999-3007.
doi: 10.1016/j.matpr.2020.10.055
63. Çelik S, Akyüz S, Özel AE. Vibrational spectroscopic characterization and structural investigations of Cepharanthine, a natural alkaloid. *J Mol Struct.* 2022;1258:132693.
doi: 10.1016/j.molstruc.2022.132693
64. Joshi A, Sharma V, Singh J, Kaushik V. Chemi-informatic approach to investigate putative pharmacoactive agents of plant origin to eradicate COVID-19. *Coronaviruses.* 2020;3(3):40-54.
doi: 10.2174/2666796701999201203210036
65. Holanda VN, Lima EMA, Silva WVD, *et al.* Identification of 1,2,3-triazole-phthalimide derivatives as potential drugs against COVID-19: A virtual screening, docking, and molecular dynamics study. *J Biomol Struct Dyn.* 2022;40(12):5462-5480.
doi: 10.1080/07391102.2020.1871073
66. Sanders JM, Monogue ML, Jodlowski TZ, Cutrell JB. Pharmacologic treatments for coronavirus disease 2019 (COVID-19): A review. *JAMA.* 2020;323(18):1824-1836.
doi: 10.1001/jama.2020.6019
67. Aziz N, Kim MY, Cho JY. Anti-inflammatory effects of luteolin: A review of *in vitro*, *in vivo*, and *in silico* studies. *J Ethnopharmacol.* 2018;225:342-358.
doi: 10.1016/j.jep.2018.05.019

Received: July 27, 2025
Revised: October 10, 2025
Accepted: November 5, 2025
Available online: November 26, 2025